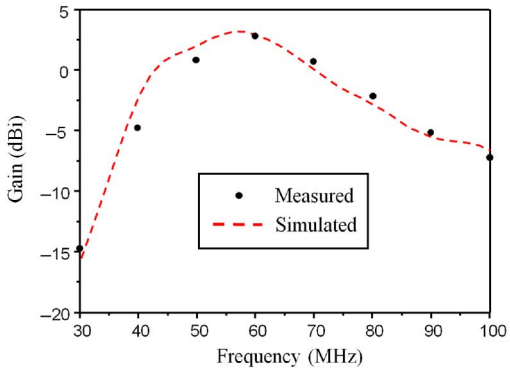

Fig. 16. Measured and simulated gain results of the dynamic-type shunt-excited sea-water monopole antenna.

However, this measurement method is very expensive and difficult to implement, which is beyond our current scope.

V. Conclusion

A shunt-excited feeding structure has been presented for dynamic-type sea-water monopole antenna. The detailed operating mechanism of the proposed shunt-excited feeding structure has been explained through an equivalent circuit model. Owing to its structural features, a high-efficiency dynamic-type sea-water monopole antenna can be readily designed. Experiments are also conducted to verify our design concept. Two prototypes of shunt-excited sea-water monopole antennas are designed and fabricated: static-type and dynamic-type. Experimental results have shown a fairly good agreement with theoretical predictions. The dynamic-type sea-water monopole antenna can be easily installed on the ship's deck or buoys. In contrast to traditional antennas, this kind of sea-water antenna can be turned OFF or tuned ON real time, which is an excellent antenna for VHF and HF maritime wireless communications.

References

[1] H. Fayad and P. Record, "Broadband liquid antenna," *Electron. Lett.*, vol. 42, no. 3, pp. 133–134, 2006.
[2] E. Paraschakis, H. Fayad, and P. Record, "Ionic liquid antenna," in *Proc. IEEE Int. Workshop Antenna Technol Small Antennas Novel Metamater.*, 2005, pp. 552–554.
[3] L. Xing, Y. Huang, S. S. Alja'afreh, and S. J. Boyes, "A monopole water antenna," in *Proc. Loughborough Antennas Propag. Conf.*, 2012, pp. 1–4.
[4] SPAWAR, "Sea Water Antenna System," SSC Pacific, San Diego, CA, Apr. 2011 [Online]. Available: http://www.public.navy.mil/spawar/Pacific/TechTransfer/ProductsServices/Pages/SeaWaterAntennaSystem.aspx and https://www.youtube.com/watch?v=9tIZUhu21sQ
[5] C. Hua, Z. Shen, and J. Lu, "High-efficiency sea-water monopole antenna for maritime wireless communications," *IEEE Trans. Antennas Propag.*, vol. 62, no. 12, pp. 5968–5973, Dec. 2014.
[6] S. Uda and Y. Mushiake, *Yagi-Uda Antennas*. Tokyo, Japan: Maruzen, 1954.
[7] E. A. Wolff, *Antenna Analysis*. Hoboken, NJ, USA: Wiley, 1966.
[8] R. W. P. King, C. W. Harrison Jr., and E. A. Aronson, "The imperfectly conducting cylindrical transmitting antenna: Numerical results," *IEEE Trans. Antennas Propag.*, vol. 14, no. 5, pp. 535–542, Sep. 1966.
[9] R. H. Johnston and J. G. McRory, "An improved small antenna radiation efficiency measurement method," *IEEE Antennas Propag. Mag.*, vol. 40, no. 5, pp. 40–48, Oct. 1998.
[10] C. A. Balanis, *Antenna Theory: Analysis and Design*. Hoboken, NJ, USA: Wiley, 2005.

Compact Single-Feed Dual-Mode Antenna for Active RFID Tag Application

Le Chang, Han Wang, Zhijun Zhang, Yue Li, and Zhenghe Feng

***Abstract*—This communication proposes a compact single-feed dual-mode antenna for active radio-frequency identification (RFID) tag application. The proposed antenna consists of a slotted patch on an FR4 substrate, a feeding microstrip line, and a foam spacer with a volume of only $60\ \text{mm} \times 50.3\ \text{mm} \times 6\ \text{mm}$ ($0.48\lambda_0 \times 0.40\lambda_0 \times 0.048\lambda_0$, where λ_0 is the wavelength at the center frequency). It operates as a dipole in free space and as a patch when placed on a metallic surface. A prototype that can provide an impedance bandwidth of 390 MHz (2.28–2.67 GHz) in free space and 470 MHz (2.32–2.79 GHz) on a metallic surface is built and measured. The measured radiation patterns, peak gains, and radiation efficiencies in these two scenarios are provided.**

***Index Terms*—Dipole antennas, patch antennas, radio-frequency identification (RFID) tags.**

I. Introduction

Radio-frequency identification (RFID) is a rapidly developing technology that provides automatic wireless identification and tracking capability. The applications of identification, tracking, automatic data acquisition, and access control make RFID technology popular in many service industries, such as distribution logistics, manufacturing companies, and goods flow systems [1]. A typical RFID system comprises a host computer, a reader, and a tag that contains information regarding the attached object. The communication link between the reader and the tag is established through wireless connection; this process is done by coupling a magnetic field or capturing an electromagnetic wave according to the communication frequency. For RFID systems operating at low-frequency (LF, 125 kHz) and high-frequency (HF, 13.65 MHz) bands, information and power are transmitted through magnetic field coupling, whereas for ultra-high-frequency (UHF, 915 MHz) and microwave (MW, 2.4 and 5.8 GHz) bands, communication is based on electromagnetic wave capture [2].

RFID systems can be grouped into two categories: 1) passive and 2) active. Passive tags do not require batteries or maintenance. They are energized by interrogation signals from the reader, and they deliver information through a backscattering-modulated signal transmitted by the reader. In passive RFID, the antenna is matched to a conjugate value [3], [4], e.g., 12-j133 Ω. Passive tags have a relatively longer lifetime than active tags. However, their reading range is limited.

Manuscript received January 23, 2015; revised June 05, 2015; accepted September 02, 2015. Date of publication September 09, 2015; date of current version October 28, 2015. This work was supported in part by the National Basic Research Program of China (contract 2013CB329002), in part by the National High Technology Research and Development Program of China (863 Program; contract 2011AA010202), in part by the National Natural Science Foundation of China (contract 61371012), in part by the National Science and Technology Major Project of the Ministry of Science and Technology of China (2013ZX03003008-002), and in part by the China Postdoctoral Science Foundation funded project (2013M530046).

The authors are with the State Key Laboratory on Microwave and Communications, Tsinghua National Laboratory for Information Science and Technology, Tsinghua University, Beijing 100084, China (e-mail: zjzh@tsinghua.edu.cn).

Color versions of one or more of the figures in this communication are available online at http://ieeexplore.ieee.org.

Digital Object Identifier 10.1109/TAP.2015.2477417

0018-926X © 2015 IEEE. Personal use is permitted, but republication/redistribution requires IEEE permission.
See http://www.ieee.org/publications_standards/publications/rights/index.html for more information.

Because passive RFIDs have limited functionality, active RFIDs were introduced. An active RFID is powered by its own battery and can carry out a lot of tasks, such as measuring temperature, humidity, vibration, and acceleration and even forming a distributed wireless ad hoc network. Communication society has studied active RFID from its own perspective for a while [5], [6]. Among the chipsets used for active RFIDs are TI CC2510 [7] and nRF24LE1 [8]. As shown in these specifications, antenna impedances of the chipsets are 50 Ω if proper matching network are used; thus, there is no need to redesign for different chips [9]–[11]. Active tags have a limited lifetime (usually 3–10 years), but their reading range is larger than that of passive tags.

A considerable challenge for both passive and active tags is their application in various environments. The most representative objects are a cardboard box (which can be considered as free space) and a metal object. In published reports, the antennas that could be used in both scenarios usually consisted of a metallic sheet [3], [12], [14]–[16] or meander lines [13], [17] and a ground plane. The ground plane was used to achieve conjugate matching, as well as to shield the metal objects when the tags were attached to a metallic surface. In passive RFID tags, the microchip was usually placed between a metallic sheet and a microstrip line with its end shorted to the ground [12]–[14]. The sheet was used to provide a current path for radiation and the microstrip line was used to generate conjugate matching with the impedance of the microchip. Feeding loops were adopted to excite a patch with two odd symmetric slots [15] and two shorted patches differentially [16]. In [3], a fork-shaped patch was used as the radiator, and two parasitic patches were used to adjust the input impedance to match various microchip impedances. The design philosophy of these metal tag antennas entailed putting a metal layer beneath the antenna in advance to shield any metal objects. A passive tag antenna without a ground structure was reported in [4]. Two different types of dipoles were used as radiating elements, and the reactances of the two structures changed in opposite directions when the tag was applied to a metallic surface; thus, the total input impedance of the antenna changed very little. However, this antenna showed a poor performance and had a relatively complex structure.

In this communication, a single-feed dual-mode active RFID tag antenna is proposed, which consists of a 50-Ω feeding microstrip line, a slotted patch on an FR4 substrate, and a foam spacer. The validity of the antenna is shown by simulation and measurement. Bandwidths of 390 MHz (2.28–2.67 GHz) and 470 MHz (2.32–2.79 GHz) are obtained, and stable peak gains and high radiation efficiencies are achieved for the dipole and patch modes, respectively.

II. Antenna Design

Fig. 1 shows the geometry of the proposed antenna, which is composed of a feeding microstrip line, a slotted patch etched on an FR4 substrate, and a foam spacer. The overall dimensions are 60 mm × 50.3 mm. The FR4 substrate has a thickness (*H1*) of 1 mm, a dielectric constant of 4.4, and a loss tangent of 0.02. As shown in Fig. 1(a), the patch has two perpendicular slots, both with a width (*Ws*) of 2 mm. The slot in the middle has a length (*Ls1*) of 25 mm; the open-ended slot etched on the edge has a length (*Ls2*) of 15 mm. Each slot is fed by an open-ended 50-Ω microstrip line. Two microstrip lines merge at the feeding point, which can be connected either to an active RFID chip or to a coaxial cable for measurement purposes, as shown in Fig. 1(a). Detailed dimensions of the proposed antenna is listed in Table I. The height (*H2*) of the foam spacer is 5 mm.

The proposed antenna has two operating modes. When placed in free space, the antenna works in the dipole mode, as shown in Fig. 2(a). In this mode, the patch is excited by the open-ended slot, and the dominant radiating currents are horizontally orientated, as depicted by the dashed line ellipse. Although strong currents exist in the center slot, these have little contribution to the radiation, as can be verified by their removal.

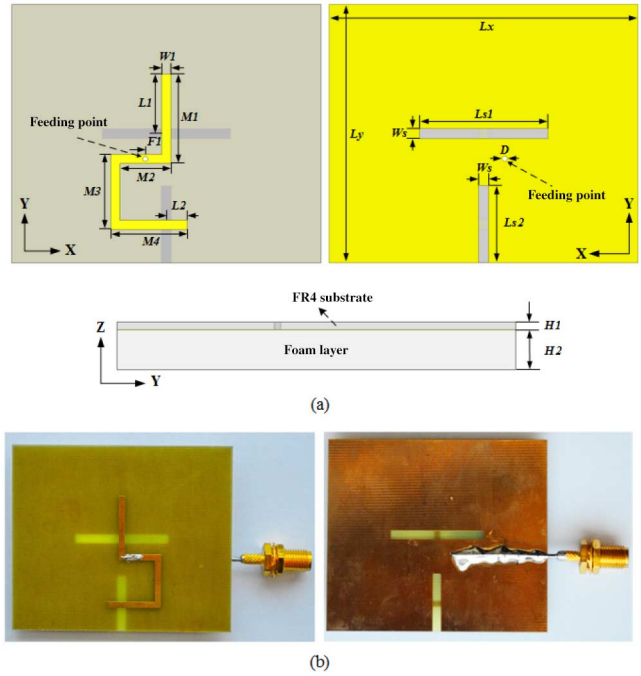

Fig. 1. Geometry of the proposed antenna and the prototype.

TABLE I
Detailed Dimensions of the Proposed Antenna

Parameter	*Lx*	*Ly*	*Ls1*	*Ls2*	*Ws*	*D*	*L1*	*W1*
Value(mm)	*60*	*50.3*	*25*	*15*	*2*	*1*	*11.6*	*1.8*
Parameter	*L2*	*H1*	*H2*	*F1*	*M1*	*M2*	*M3*	*M4*
Value(mm)	*4*	*1*	*5*	*3.2*	*17.4*	*9.9*	*14.65*	*14.8*

When placed on a metal surface, the antenna works in the patch mode. A square ground plane with dimensions of 120 mm × 120 mm is used here for design purposes; the impact of the generalized ground is parametrically studied later in this work. Fig. 2(b) shows the current distribution in the patch mode. In this mode, the antenna is excited by the center slot and functions as a conventional 5 mm-thick patch antenna.

The design procedure of the proposed antenna is described as follows. First, designing a conventional 5 mm-thick slotted patch antenna on a ground plane. A 50-Ω microstrip line, referred to as line-1, is used to excite the patch through the slot. Second, removing the ground plane; this will cause the antenna impedance mismatch. Then, adjusting the length of line-1; this transmission line can rotate the mismatched antenna impedance on a Smith Chart. The goal is to move the impedance as close as possible to the open circuit spot.

Next, leaving the antenna in free space, cutting a slot on the edge of the existing patch, and using a separate 50-Ω microstrip line, referred to as line-2, to feed the slot. The dipole mode can be excited by the new slot. In this mode, the antenna can be tuned by the length of the slot (*Ls2*) and the open-ended microstrip line (*L2*). After tuning, putting the dipole-mode antenna back on a metal surface; the antenna impedance at line-2 will be mismatched. Then, adjusting the length of line-2, and moving its impedance as close as possible to the open circuit spot.

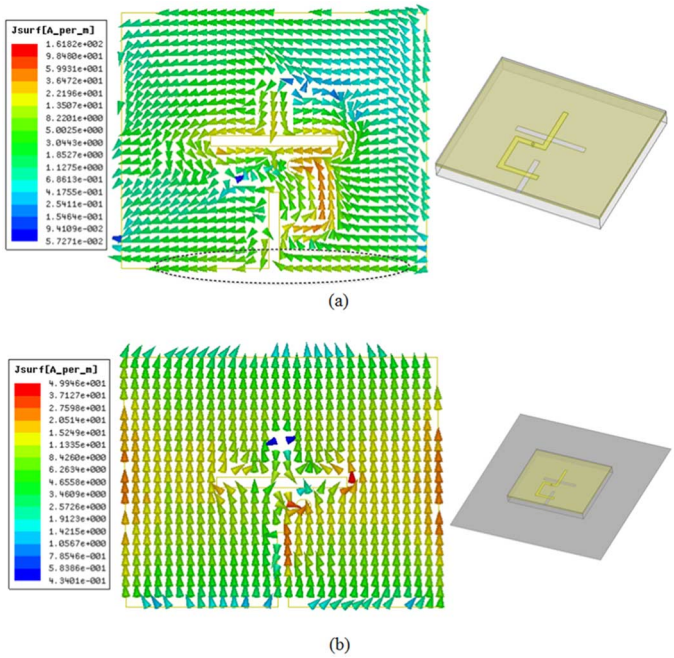

Fig. 2. Current distributions of the two operating modes at 2.4 GHz. (a) Dipole mode in free space. (b) Patch mode on a metallic surface.

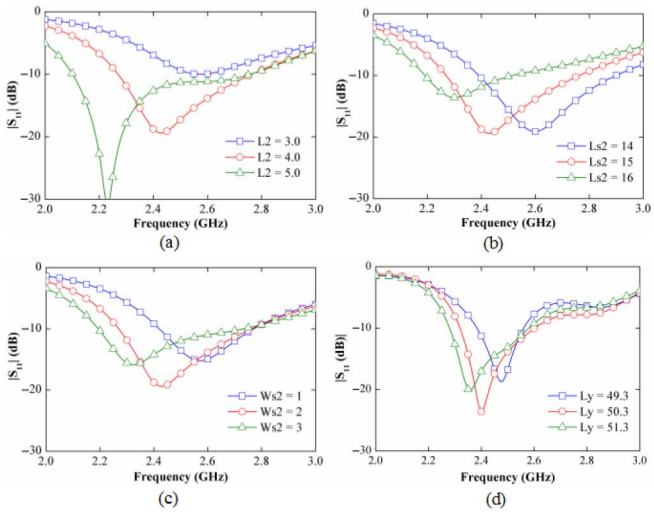

Fig. 3. Magnitude of reflection coefficients with variation of (a) *L2*, (b) *Ls2*, (c) *Ws2* for the dipole mode, and (d) *Ly* for the patch mode (unit: millimeter).

As a final step, merging line-1 and line-2. The absolute lengths of both lines must be maintained at this stage. When placed on a metal surface, the line-1 side of the finished antenna will be matched, and its line-2 side will be an open circuit; thus, only the patch mode can be excited. In free space, the line-2 side will be matched, and only the dipole mode can be excited.

Some key parameters that have significant effects on the antenna performance are studied. In these parametric studies, only one parameter at a time is adjusted; the others are kept invariant.

L2 is an important parameter of impedance matching in the dipole mode. Fig. 3(a) shows the effects as L2 varies from 3 to 5 mm in the dipole mode; the optimized length of $L2 = 4$ mm is selected for best matching. The length and width of the vertical slot have a considerable influence on the resonant frequency in the dipole mode,

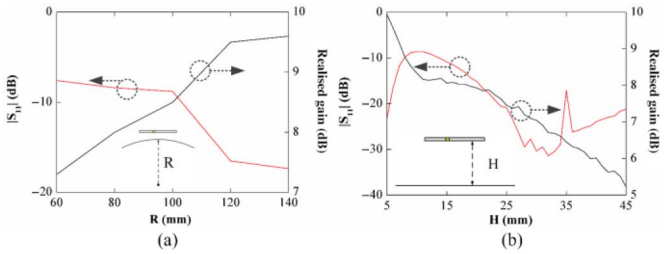

Fig. 4. Magnitude of reflection coefficients and realized gains at broadside at 2.4 GHz with variation of (a) R and (b) H.

as shown in Fig. 3(b) and (c). When the length and width increase from 14 to 16 mm and 1 to 3 mm, respectively, the resonant frequency decreases. This is because the increase in length and width extends the current path. The optimized values for good matching are $Ls2 = 15$ mm and $Ws = 2$ mm. In the patch mode, the operating frequency is determined by the length of Ly. Fig. 3(d) indicates that with the increase in Ly, the resonant frequency decreases; an optimized length of $Ly = 50.3$ mm is selected for good impedance matching at 2.4 GHz.

Because the RFID tag will be attached to various metallic objects, the impacts of ground shape and distance to ground are studied. First, the ground plane, which has dimensions of 120 mm $\times$ 120 mm, is winded on a cylinder with radius R to imitate a curved surface. As shown in Fig. 4(a), when R decreases from 140 to 60 mm, the reflection coefficients are -17.38, -16.5, -8.8, -8.4, and -7.6 dB, respectively, and the realized gains at broadside are 9.6, 9.5, 8.5, 8.0, and 7.3 dB, respectively. Even in the worst case of $R = 60$ mm, the proposed antenna has an acceptable performance.

Second, as shown in Fig. 4(b), when the distance between the proposed antenna and the ground plane is increased from 5 to 45 mm, the reflection coefficient at 2.4 GHz is better than -8.6 dB. The realized gain at broadside decreases monotonously with the increase in distance. With increasing distance between the patch and the ground plane, a hybrid mode, which is a mixture of the patch mode and the dipole mode, is excited. Thus, the realized gain is between that of the patch mode and the dipole mode. This indicates that the performance of the proposed antenna is rather robust.

III. Antenna Fabrication and Measurement Results

A prototype of the proposed antenna is fabricated, as shown in Fig. 1(b). The foam spacer is removed to show clearly the connection between the coaxial cable, which is used to carry out measurements, and the patch. The inner conductor of the coaxial line is soldered to the microstrip line, and the outer conductor is soldered to the patch. The performances of the antenna in free space and on a metallic surface are measured. The square ground plane described in Section II is not shown here. The return loss is measured with an Agilent E5071B vector network analyzer, and the radiation patterns, peak gains, and radiation efficiencies are obtained in an anechoic chamber.

Fig. 5 shows the measured reflection coefficients of the proposed antenna in comparison with the simulated results. The measurements agree well with the simulation results under the two working conditions. The measured and simulated impedance bandwidths are 390 MHz (2.28–2.67 GHz) and 530 MHz (2.24–2.77 GHz), respectively, in the dipole mode; and 470 MHz (2.32–2.79 GHz) and 270 MHz (2.31–2.58 GHz), respectively, in the patch mode.

The measured and simulated normalized total gain patterns at 2.4 GHz in free space are plotted in Fig. 6(a) and (b). As shown in the figure, the proposed antenna has bidirectional patterns in free space,

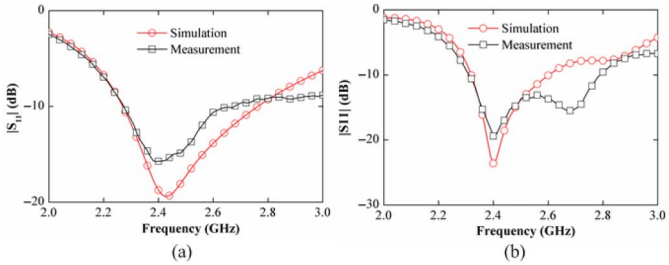

Fig. 5. Measured and simulated magnitude of reflection coefficients of the proposed antenna. (a) Dipole mode. (b) Patch mode.

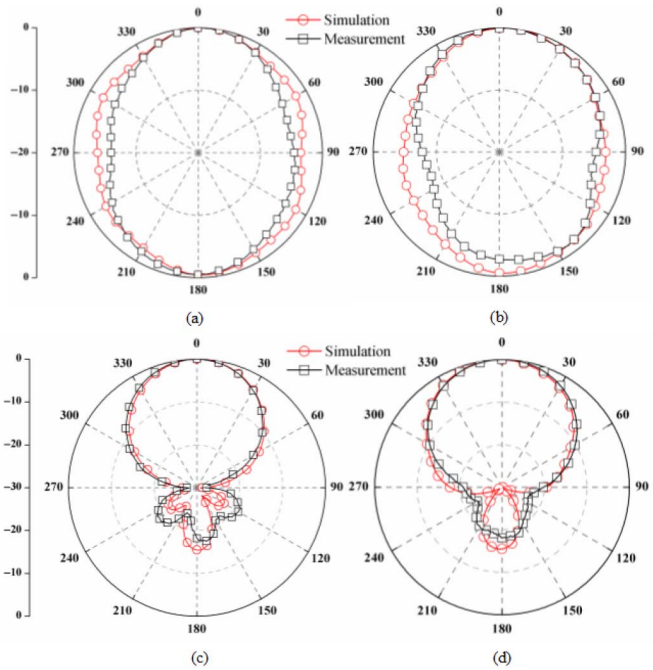

Fig. 6. Measured and simulated radiation patterns of the proposed antenna at 2.4 GHz: the dipole mode in (a) E-plane and (b) H-plane, and the patch mode in (c) E-plane and (d) H-plane.

and the patterns are near-omnidirectional in the E-(XZ) and H-(YZ) planes. The maximum directions are $\theta = 2^\circ$ and $\theta = 8^\circ$ in the E- and H-planes, respectively. Fig. 7(a) shows the measured and simulated peak gains, which at 2.4 GHz are 2.16 and 2.54 dB, respectively. The measured and simulated normalized total gain patterns at 2.4 GHz in the E-(YZ) and H-(XZ) planes when the proposed antenna is applied on a metal surface are plotted in Fig. 6(c) and (d), which shows classic radiation patterns in the patch mode. As shown in Fig. 7(a), the peak gains at 2.4 GHz are 9.36 dB in the measurement and 9.93 dB in the simulation. These results indicate that the measured and simulated patterns are in good agreement with each other.

Fig. 7 presents the measured and simulated peak gains and radiation efficiencies of the proposed antenna. As shown in the plot, the measured peak gains in the passband in the dipole mode are between 1.99 and 2.66 dB, whereas the simulated results are between 2.37 and 2.7 dB. The measured peak gains in the patch mode are between 9.32 and 9.93 dB, whereas the simulated results are between 8.42 and 9.42 dB. The measured efficiencies in the dipole and the patch mode range from 84% to 94% and 82% to 97%, respectively, whereas the simulated results are from 86% to 93% and 83% to 99%, respectively. The small deviation between the measured and simulated results is attributed to fabrication and measurement errors.

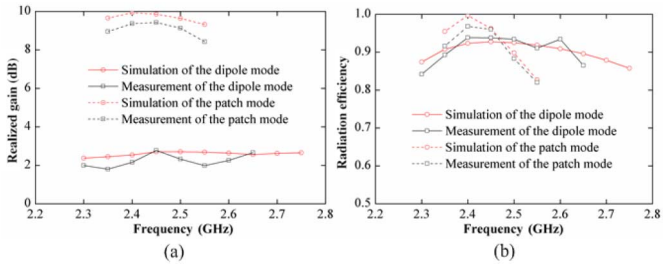

Fig. 7. Measured and simulated (a) peak gains and (b) radiation efficiencies of the proposed antenna.

As discussed above, the agreements in reflection coefficients, radiation patterns, peak gains, and radiation efficiencies between the measurement and the simulation demonstrate the feasibility of the dual-mode property. Therefore, the proposed antenna can be applied either on a cardboard box or metallic surface.

IV. Conclusion

A single-feed dual-mode active RFID tag antenna that operates in the microwave frequency is proposed. The dual-mode function is achieved by having one mode with matched impedance and the other mode with infinite input impedance under two scenarios. When used in free space, the antenna functions as a dipole; when applied on a metallic surface, it functions as a patch. What distinguishes the proposed antenna from previous dual-application RFID tag antennas is that its structure contains no ground plane. The prototype showed the potential application and good performance of the proposed design.

References

[1] K. Finkenzeller, *RFID Handbook*, 2nd ed. Hoboken, NY, USA: Wiley, 2004.

[2] P. Hajizadeh, H. R. Hassani, and S. H. Sedighy, "Planar artificial transmission lines loading for miniaturization of RFID printed Quasi-Yagi antenna," *IEEE Antennas Wireless Propag. Lett.*, vol. 12, pp. 464–467, Mar. 2013.

[3] K. H. Kim, J. G. Song, D. H. Kim, H. S. Hu, and J. H. Park, "Fork-shaped RFID tag mountable on metallic surfaces," *Electron. Lett.*, vol. 43, pp. 1400–1402, Dec. 2007.

[4] C. Cho, H. Choo, and I. Park, "Design of planar RFID tag antenna for metallic objects," *Electron. Lett.*, vol. 44, no. 3, pp. 175–177, Dec. 2008.

[5] H. Cho, J. Kim, and Y. Baek, "Large-scale active RFID system utilizing ZigBee networks," *IEEE Trans. Consum. Electron.*, vol. 57, no. 2, pp. 379–385, May 2011.

[6] W. J. Yoon and S. H. Chung, "ISS-TCA: An identified slot scan-based tag collection algorithm for performance improvement in active RFID systems," *IEEE Trans. Ind. Electron.*, vol. 59, no. 3, pp. 1662–1672, Mar. 2012.

[7] Texas Instruments. (2015). Dallas, Texas [Online]. Available: http://www.ti.com.cn/cn/lit/ds/symlink/cc2510.pdf

[8] Nordic Semiconductor. (2010, Aug.). Trondheim, Norway [Online]. Available: http://www.nordicsemi.com/eng/content/download/2443/29442/file/nRF24LE1_Product_Specification_rev1_6.pdf

[9] L. Liang and S. V. Hum, "A low-profile antenna with quasi-isotropic pattern for UHF RFID applications," *IEEE Antennas Wireless Propag. Lett.*, vol. 12, pp. 210–213, Feb. 2013.

[10] L. Pazin, A. Dyskin, and Y. Leviatan, "Quasi-isotropic X-band inverted-F antenna for active RFID tags," *IEEE Antennas Wireless Propag. Lett.*, vol. 8, pp. 27–29, Dec. 2009.

[11] Z. Fang, R. Jin, and J. Geng, "Asymmetric dipole antenna suitable for active RFID tags," *Electron. Lett.*, vol. 44, no. 2, pp. 71–72, Jan. 2008.

[12] J. H. Lu and K. T. Hung, "Planar inverted-E antenna for UHF RFID tag on metallic objects with bandwidth enhancement," *Electron. Lett.*, vol. 46, pp. 1182–1183, Aug. 2010.

[13] J.-H. Lu and G.-T. Zheng, "Planar broadband tag antenna mounted on the metallic material for UHF RFID system," *IEEE Antennas Wireless Propag. Lett.*, vol. 10, pp. 1405–1408, Dec. 2011.
[14] B. Lee and B. Yu, "Compact structure of UHF band RFID tag antenna mountable on metallic objects," *Microw. Opt. Technol. Lett.*, vol. 50, no. 1, pp. 232–234, Jan. 2008.
[15] Z. Zhang and X. Liu, "A low-profile planar broadband UHF RFID tag antenna for metallic objects," in *Proc. Int. Symp. Antennas Propag. (ISAP'13)*, Oct. 2013, vol. 2, pp. 1162–1165.
[16] B. Yu, S. Kim, B. Jung, F. Harackiewicz, and B. Lee, "RFID tag antenna using two-shorted microstrip patches mountable on metallic objects," *Microw. Opt. Technol. Lett.*, vol. 49, no. 20, pp. 414–416, Feb. 2007.
[17] H. D. Chen and Y. H. Tsao, "Broadband capacitively coupled patch antenna for RFID tag mountable on metallic objects," *IEEE Antennas Wireless Propag. Lett.*, vol. 9, pp. 489–492, May 2010.

Circular Polarization Frequency Selective Surface Operating in Ku and Ka Band

Robert Orr, Vincent Fusco, Dmitry Zelenchuk, George Goussetis, Elena Saenz, Massimiliano Simeoni, and Luca Salghetti Drioli

***Abstract*—A double layer circular polarization (CP) frequency selective surface (FSS) for use as a dual-band quasi-optical diplexer suitable for deployment in reflector antenna systems is described. The FSS was designed to reflect Ku band signals (11.7–12.75 GHz) while transmitting Ka band signals (17.3–20.2 GHz) and conserving CP in each of these bands. The simulated/measured reflection loss over the Ku band was less than 0.05/0.1 dB for both TE and TM polarizations, while the simulated/measured axial ratio was less than 0.2/0.75 dB. Over the Ka band, the simulated/measured transmission loss for both polarizations was below 0.25/0.4 dB and the simulated/measured axial ratio was less than 0.25/0.75 dB. To the best of our knowledge, this is the first report of a metallo-dielectric FSS that simultaneously operates in CP for an oblique angle of incidence in both Ku and Ka bands.**

***Index Terms*—Circular polarized FSS, Ka–Ku band, satellite communications.**

I. Introduction

Frequency selective surfaces (FSSs) have been used as frequency diplexers in satellite reflector antenna systems with feeds placed on either side of the FSS [1]–[3]. In this configuration, the FSS is designed to be reflective for one of the feeds, thus acting as a subreflector, while for the other it is transparent allowing the feed to be placed at the focal point of the main reflector, see Fig. 1. Both feed antennas can, therefore, utilize the same main reflector. This is a method by which the communication capacity of the antenna system can be increased while reducing the mass and volume of the satellite payload.

The recent trend in satellite systems is toward operation in circular polarization (CP), which is advantageous in communication and sensing systems as it provides resilience to effects such as Faraday rotation [4] and rain clutter [5] while also removing the requirement for polarization alignment between the transmitter and receiver. In conjunction with the ever increasing demand for higher throughput, as, e.g., highlighted by the trend toward multibeam satellite communications coverage, these developments bring to fore the need for a quasi-optical FSS diplexer that operates in CP as identified in [6].

Recently, there has been much interest in the design of polarization independent FSSs. These surfaces have near identical reflection and transmission coefficient magnitudes for TE and TM polarized waves. Several FSS geometries with such properties have been presented including crossed dipoles [7], Jerusalem cross apertures [8], conducting rings [9], double square loop arrays, and gridded double square loop arrays [10]. FSS consisting of an array of nested slots has recently been developed for the detection of dual-polarized radiation in passive remote sensing space science instruments [11], [12]. Such FSS elements made up of a pair of nested shorted annular slots allow independent control of the spectral response for TE and TM polarizations at oblique angles of incidence.

In a CP quasi-optical diplexer, CP should be maintained in both the reflection and transmission bands. Consequently, the FSS reflection/transmission coefficient (both magnitude and phase) should be equal for the TE and TM polarizations. For plane waves incident in the direction normal to a planar FSS, the geometrical symmetry ensures coincident magnitude and phase responses for the two principal linear polarizations. However, the symmetry breaks for the case of obliquely incidence waves, as would be required to address the scenario depicted in Fig. 1. While the designs in [7]–[12] focus on ensuring that reflection and transmission magnitude are equal for obliquely incident TE and TM polarized waves, their phase properties are not considered, and therefore, the conservation of CP upon reflection and transmission cannot be guaranteed.

In this communication, we report the first metallo-dielectric FSS that operates in CP. The presented FSS design is suitable for use as a quasi-optical CP diplexer and meets the typical frequency plan of a modern satellite communication system. In particular, the FSS reflects signals occurring in the Ku band (11.7–12.75 GHz) and transmits those in the Ka band (17.3–20.2 GHz). Conservation of the CP signal is achieved simultaneously in both the reflection/transmission bands by ensuring that the reflection/transmission magnitude and phase are as near equal as possible for TE and TM polarizations over the respective operating bands.

II. Simulated and Measurement Results

Double square loop FSS elements [13]–[15] were utilized in the FSS design. This element type was favored as it allows for independent tuning of the reflection and transmission bands by modifying the dimensions of the relevant loop. Furthermore, they provide good angular stability and allow the elements to be packed closely together with enhanced bandwidth. Our investigations (not shown here for brevity) have demonstrated that although single layer FSS designs can produce CP response, the bandwidths that they can achieve are too narrow for

Manuscript received January 08, 2015; revised April 28, 2015; accepted September 02, 2015. Date of publication September 09, 2015; date of current version October 28, 2015. This work was supported in part by the European Space Agency under Grant 4000105324/12/NL/NR and in part by the Department of Employment and Learning (DEL) Northern Ireland.

R. Orr, V. Fusco, and D. Zelenchuk are with the Institute of Electronics Communications and Information Technology, Queens University Belfast, Belfast BT3 9DT, U.K. (e-mail: rorr08@qub.ac.uk; v.fusco@ecit.qub.ac.uk; d.zelenchuk@qub.ac.uk).

G. Goussetis is with Heriot-Watt University, Edinburgh EH14 4AS, U.K. (e-mail: g.goussetis@ieee.org).

E. Saenz, M. Simeoni, and L. Salghetti Drioli are with the European Space Agency, ESA-ESTEC, 2200 AG Noordwijk, The Netherlands (e-mail: elena.saenz@esa.int; massimiliano.simeoni@esa.int; luca.salghetti.drioli@esa.int).

Color versions of one or more of the figures in this communication are available online at http://ieeexplore.ieee.org.

Digital Object Identifier 10.1109/TAP.2015.2477519

0018-926X © 2015 IEEE. Personal use is permitted, but republication/redistribution requires IEEE permission.
See http://www.ieee.org/publications_standards/publications/rights/index.html for more information.